

Enhanced photothermal cooling of nanowires

G. Guccione¹, M. Hosseini², A. Mirzaei³, H. J. Slatyer¹, B. C. Buchler¹, and
P. K. Lam^{*1}

¹*Centre for Quantum Computation and Communication Technology, Department of Quantum Science, Research School of Physics and Engineering, The Australian National University, Canberra ACT 2601, Australia*

²*Birck Nanotechnology Center, School of Electrical and Computer Engineering, Purdue University, West Lafayette, Indiana 47907, USA*

³*Nonlinear Physics Centre, Research School of Physics and Engineering, The Australian National University, Canberra ACT 2601, Australia*

March 17, 2022

Abstract

We investigate the optomechanical interaction between light and metallic nanowires through the action of bolometric forces. We show that the response time of the photothermal forces induced on the nanowire is fast and the strength of the interaction can overcome the radiation pressure force. Furthermore, we suggest the photothermal forces can be enhanced by surface plasmon excitation to cool the sub-megahertz vibrational modes of the nanowires close to its quantum limit.

1 Introduction

Micro- and nanoscale oscillators have attracted significant attention for sensing applications thanks to their small masses and therefore an extreme sensitivity to the external drives [1]. To date, nanomechanical devices are used to perform ultra-sensitive measurements of, for example, biological material properties [2], mass sensing at the level of single particles and molecules [3, 4, 5, 6], and sub-attoneutron force sensing [7]. Other fields benefitting from the incredible resolution of nanomechanical sensors include

*Ping.Lam@anu.edu.au

accelerometry [8], charge sensing [9], and magnetometry, with tremendous implications for three-dimensional imaging thanks to the resolution at the level of a single electronic spin [10]. With interest growing in several areas, and the availability of faster, cheaper, and more precise fabrication techniques, nanoscopic probes are now established for ultra-fast, high-precision sensing in a variety of applications [11].

To push beyond the classical boundaries of sensitivity, the sensors need to operate in the quantum regime. The major challenge is usually represented by the coupling of the system with a thermal environment that hides or even destroys the quantum characteristics of the object. A careful control of the interaction between the sensor and its thermal bath is the key to observing quantum behaviour, especially in the case of mesoscopic objects. Optomechanical systems have been considered recently as viable platforms for revealing the quantum nature of mechanical oscillators at the mesoscale [12, 13, 14]. Optomechanics allows the coherent and controllable exchange of photonic and phononic excitations and presents a viable option for the neutralization of the incoherent thermal drive of the oscillator. The collective motion of billions of atoms can be regulated by laser light to reveal the quantum properties of the mechanical system. This optomechanics-induced control has been proven to expose the quantum nature of the oscillators by cooling nanomechanical resonators to their quantum ground state (QGS) [15, 16, 17], by generating optomechanical squeezing [18, 19, 20], and by achieving quantum state transfer between hybrid systems [14, 21].

The first requirement for achieving pure quantum mechanical states of motion is that the mode of vibration be cooled into the QGS by extracting all the energy from the phononic mode and by providing adequate isolation from environmental decoherence. It is, therefore, crucial to be able to control [22] and characterize the mechanical motion at a level below Heisenberg's uncertainty limit [23]. The first QGS cooling experiment was performed on a nano-oscillator with a mechanical frequency of 6 GHz [15]. A general condition for the achievement of the QGS is that the optomechanical system exhibit ultra-high optical and mechanical quality factors. One of the present challenges in the field of cavity optomechanics is to cool the modes of mechanical resonators with smaller frequencies of oscillations to the quantum regime as it entails the fabrication of devices that are not easily accessible with the current technology. For example, the linewidth of the optical resonator might be required on the order of kilohertz or lower. Even if such narrow-band resonators were attained, the interaction bandwidth would be extremely reduced as a result. Very recently, it was proposed that the quantum regime of a specially designed high-stress silicon nitride mem-

brane with sub-megahertz vibration frequency can in principle be reached thanks to the remarkably low mechanical dissipation in such structures [24].

In this paper, we study an alternative and unconventional approach to the cooling of an oscillator with sub-megahertz vibrational frequencies near the QGS. We suggest the use of metallic nanowires driven by photothermal forces [25, 26], which can be subject to the excitation of plasmonic modes to amplify the interaction between the optical and the mechanical modes. The enhanced photothermal forces can be used to effectively cool nano-sensors without the need for cavity sideband cooling. The tight-light confinement beyond the diffraction limit provided by plasmonic resonances thus enables strong and broadband optomechanical interaction which can be used to probe the quantum limits of photothermal cooling [27, 28].

2 Metallic nanowires as mechanical oscillators

The investigations on methods to boost the force sensitivity of nano-probes discussed throughout this paper involve the use of commercial crystalline nanowires¹. Each nanowire is grown coaxially at the extremity of a tungsten needle, by a process that involves dipping of the silver-coated tip of the needle into a droplet of liquid gallium at room temperature. Slow retraction of the tip from the droplet allows the two metals to alloy into a long, uniform rod of Ag₂Ga crystallites [29] (cf. Fig. 1).

Similar nanowires have been used to quantify the surface tension, the viscosity, and other properties of fluids at the microscopic level [30], and to perform high-precision subsurface characterization of nano-structures with high dielectric constants [31]. Visual force sensing was also demonstrated by directly monitoring their buckling deformations [32]. In biology, they have been considered for the detection of edge-binding effects in proteins [33]. In most applications, however, the quality of the measurements in ordinary operating environments is compromised by the thermally induced vibrations of the nanowires. The laser cooling method described here can boost the sensitivity of the nanowires during the transient dynamics of the oscillations [34].

The self-assembled Ag₂Ga nanowires have a relatively wide range of specifications, summarized in Table 1. They range in size between 20 and 60 μm in length and between 50 and 200 nm in diameter. To push up the detection efficiency of their vibrational modes, which depends on the light scattered from their surface, a number of specimens were coated with about 50 nm of gold.

¹NN-NCL from NaugaNeedles LLC [<http://nauganeedles.com/>]

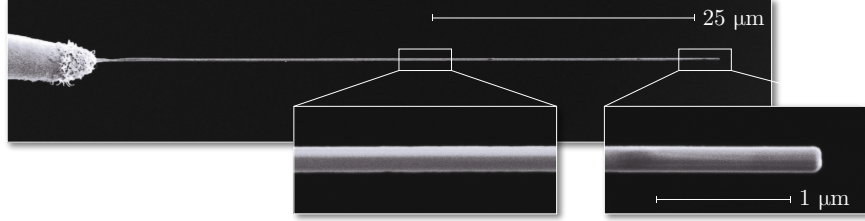


Figure 1: Images of a nanowire, obtained by scanning electron microscopy. The images in the insets show close-ups of the nanowire structure along the shaft and at the tip.

The quality factor Q determines the capability of the system to store energy into the oscillations. It is defined as the ratio of the total energy divided by the energy lost over one cycle. Generally, the quality factor is strongly influenced by a variety of elements, such as thermoelastic and mechanical properties of the oscillator and its support, and the viscosity of the surrounding medium. For a mechanical oscillator where intrinsic mechanical damping and air viscosity are the main factors contributing to the dissipation, the quality factor Q can be expressed as

$$Q = \left(Q_m^{-1} + Q_{\text{air}}^{-1} \right)^{-1}, \quad (1)$$

where $Q_m = \omega_m / \gamma_m$ and $Q_{\text{air}} = \omega_m / \gamma_{\text{air}}$ are the ratio of the oscillator's eigenfrequency and the damping rate due to the intrinsic mechanical losses or due to the air, respectively. The contribution of air viscosity in ordinary

Quantity	Value
Length	20–60 μm
Diameter	50–200 nm (coated: 90–500 nm)
Density	8960 kg m^{-3}
Mass	1–70 pg (coated: 4–150 pg)
Oscillation frequency	20–500 kHz (fundamental)
Stiffness	0.1–10 mN m^{-1} (fundamental)
Elastic modulus	≈ 100 GPa
Damping rate	0.5–0.9 kHz (in air: ≈ 10 kHz)

Table 1: Typical characteristics of the Ag_2Ga nanowires used in the experiments.

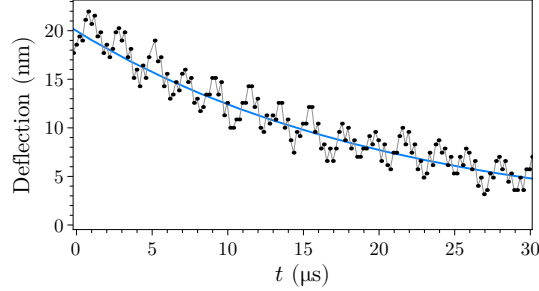


Figure 2: Time-domain measurement of the relaxation rate of a nanowire in air. The nanowire ($\approx 50 \mu\text{m}$ long, $\approx 300 \text{ nm}$ thick) is subject to a thermally induced deflection until $t = 0$, at which point the amplitude of the deflection undergoes exponential decay to the original state. The high-frequency fluctuations on top of the decay represent oscillations at the mechanical frequency. For this specimen the rate obtained by exponential fit of the moving average (solid blue line) is $7.6(4) \text{ kHz}$.

atmospheric conditions is typically dominating for most high-quality resonators [35], saturating the quality factor to a value that can be estimated by

$$Q_{\text{air}}^{(\text{atm})} = \frac{2\alpha^2}{\mu_{\text{air}} C_d l^2} \sqrt{\rho A Y I}, \quad (2)$$

where l is the length of the cylinder, A is the cross-sectional area, ρ is the density, Y is the elastic modulus, I is the areal moment, α is a mode-dependent coefficient which is respectively equal to 1.87510 and 4.69409 for the first two eigenmodes [36], μ_{air} is the dynamic viscosity of air, and C_d is the drag coefficient, a function of the Reynolds number and of the oscillator's geometry. By transferring the oscillator into vacuum, the lower density of air molecules is such that they interact with the system without further collisions amongst each other. As more air is pumped out, background gas collisions decrease and the quality factor becomes inversely proportional to the pressure P [37]:

$$Q_{\text{air}}^{(\text{vac})} = \sqrt{\frac{\pi}{2} \frac{RT}{M_{\text{air}}}} \frac{\alpha^2 r}{2l^2} \sqrt{\frac{\rho Y I}{A} \frac{1}{P}}, \quad (3)$$

where R is the universal gas constant, T the temperature, and M_{air} the molar mass of air. The quality factor cannot be increased arbitrarily, however. At some point further reduction of background gas collisions will have little

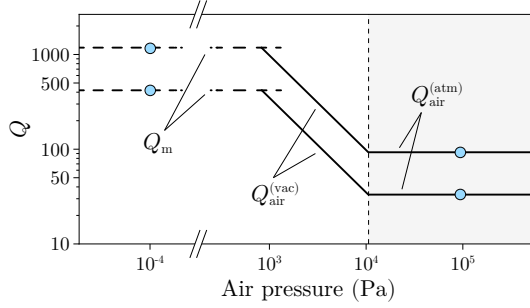


Figure 3: Quality factor of two different oscillation modes in air and in vacuum conditions. The circles correspond to the quality factor obtained by dividing the first two eigenfrequencies of the nanowire by the corresponding damping rates, empirically measured to be ≈ 10 kHz in air and ≈ 0.8 kHz in high vacuum for a nanowire with similar eigenfrequencies. The solid lines indicate the quality factor, dominated by air dissipation, which is expected by the model for a nanowire at room temperature ($T = 300$ K) with elastic modulus $Y = 85$ GPa, density $\rho = 8960$ kg m $^{-3}$, diameter $2r = 200$ nm, and length $l = 40$ μ m. The molar mass used in the model in the high-pressure regime is $M_{\text{air}} = 28.97 \times 10^{-3}$ kg mol $^{-1}$, and the air viscosity required in the high-pressure regime is $\mu_{\text{air}} = 1.8 \times 10^{-5}$ Pa s. The drag coefficient C_d , estimated to be between 1 and 10 for a cylinder with Reynolds number around unity, was fitted to a value of 2.0. The transition between the regime of individual gas collisions and viscous dynamics is, for these parameters, around 10.5 kPa. The intrinsic mechanical dissipation takes over at pressures lower than one kilopascal.

or no effect, as other intrinsic damping attributes prevail. As these are often specific to the manufacturing process or other details not always easily accessible [37, 1], it is hard to predict what is the highest quality factor achievable by the apparatus without a direct measurement. The decay rates of the thermally excited oscillations of the nanowires in air, measured from the linewidth of the resonances on the spectrum analyser, was observed to be around 10 kHz due to the interaction with gas molecules (cf. Fig. 2). This corresponds to quality factors of up to 50 for the fundamental modes. Insertion of the nanowires in a vacuum chamber reduced the damping rates to less than 1 kHz, pushing the quality factors to 500 or more (cf. Fig. 3). When operating in vacuum, the damping rate of the nanowires was inferred from the time domain evolution of the oscillations to overcome the limit in resolution bandwidth of the spectrum analyser. The chamber was operated in high-vacuum conditions at pressures of 10^{-4} Pa or lower to avoid air

having any role in the damping mechanism.

3 Scattering and detection

Optical measurements play an important role in the detection of small movements of the nanostructures. Light confinement is important to enhance the read-out efficiency. Nanophotonic crystal waveguides [38] and cavities [39] are widely used in applications that require a tight confinement of the optical mode. Very recently, it was demonstrated that a coupling efficiency for spontaneous emission exceeding 85 % can be achieved when a single carbon nanotube is coupled to a silicon photonic crystal nanobeam cavity with an ultra-low mode volume [40]. Coupling of this strength significantly improves light-matter interactions and enables precise control and read-out, crucial qualities for quantum information and sensing. The light confinement in these systems is however limited by diffraction, which prevents sub-wavelength confinement in the nanophotonic structures. When dealing with objects of 100 nm in radius, effects at the sub-wavelength scale become a significant and inherent part of the system. In this regime radiation pressure is dominated by scattering forces, leading to losses and decreasing the capacity of interaction with the oscillator.

To model the scattering of the metallic nanowires, we follow Mie scattering theory for a sub-wavelength cylinder [41]. The solutions are expressed in terms of infinite series of the scattering coefficients $\{c_n\}_{n \in \mathbb{N}}$, whose value strongly depends on the geometry and refractive index of the object as well as the polarization and the angle of incidence of the field. Notably, any display of absorption is derived from a propagation of the imaginary part of the complex refractive index of the material. We limit our analysis to the case of light normally incident to the axis of the nanowire, with beam width W much larger than the cross-sectional dimensions, i.e. $W \gg r$ with r being the radius of the cylinder. The angular distribution of the scattered field is

$$E_{\text{sca}}(\phi) = \sqrt{\frac{2}{\pi\xi}} e^{i(\frac{3\pi}{4} + \xi)} T(\phi) E_{\text{in}}, \quad (4)$$

where ϕ is the polar angle, $\xi = 2\pi r/\lambda$ is a dimensionless ratio between the characteristic length of the object and the wavelength, and E_{in} is simply the input field. The dependence on the refractive index of the object is implicit in the transfer coefficient $T(\phi)$, which is determined by the scattering

coefficients as

$$T(\phi) = c_0 + 2 \sum_{n=1}^{+\infty} c_n \cos(n(\pi - \phi)). \quad (5)$$

The extinction, scattering, and absorption efficiencies, equivalent to the ratio between the effective cross section of each process and the cross-sectional area of the target, are also calculable from the scattering coefficients. They are

$$q_{\text{ext}} = \frac{2}{\xi} \left(\Re(c_0) + 2 \sum_{n=1}^{+\infty} \Re(c_n) \right), \quad (6)$$

$$q_{\text{sca}} = \frac{2}{\xi} \left(|c_0|^2 + 2 \sum_{n=1}^{+\infty} |c_n|^2 \right), \quad (7)$$

$$q_{\text{abs}} = q_{\text{ext}} - q_{\text{sca}}. \quad (8)$$

It should be specified that, despite their name, these efficiencies are not bound to unity in Mie scattering theory. As a matter of fact, in many examples the light scattered or absorbed is more than that geometrically incident on the object [41]. The efficiencies are needed to infer the amount of radiation pressure force contributing to each process [42]. We have that the scattering and absorption components of radiation pressure force are respectively

$$F_{\text{sca}} = \frac{q_{\text{sca}} P_{\text{in}}}{c}, \quad (9)$$

$$F_{\text{abs}} = \frac{q_{\text{abs}} P_{\text{in}}}{c}, \quad (10)$$

in terms of the incident power P_{in} , which is calculated by integrating the intensity of the beam over the irradiated cross-sectional area of the cylinder projected onto the plane perpendicular to the propagation of the field [43]. The scattering coefficients are the only elements needed to calculate all of these quantities that are still unspecified. The reason lies in the fact that their definition differs depending on whether the polarization of the field is parallel or perpendicular to the cylinder's axis:

$$c_n = \begin{cases} \frac{J_n(\nu\xi)J'_n(\xi) - \nu J'_n(\nu\xi)J_n(\xi)}{J_n(\nu\xi)H'_n{}^1(\xi) - \nu J'_n(\nu\xi)H_n^1(\xi)} & \text{for parallel polarization,} \\ \frac{\nu J_n(\nu\xi)J'_n(\xi) - J'_n(\nu\xi)J_n(\xi)}{\nu J_n(\nu\xi)H'_n{}^1(\xi) - J'_n(\nu\xi)H_n^1(\xi)} & \text{for perpendicular polarization.} \end{cases} \quad (11)$$

Here, $\nu = n_{\text{nw}}/n_0$ is the ratio between the refractive index of the cylindrical nanowire, n_{nw} , and the one of the surrounding medium, n_0 . The functions $\{J_n\}_{n \in \mathbb{N}}$ are the Bessel functions of the first kind and $\{H_n^1\}_{n \in \mathbb{N}}$ are the Hankel functions of the first kind. The prime indicates differentiation relative to the full argument of the relative function. The derivatives for both classes of functions can be easily computed as the halved difference of the involved functions with preceding and succeeding indices, e.g. $J'_n(x) = (J_{n-1}(x) - J_{n+1}(x))/2$. For any other polarization the result is obtained by the appropriate linear combination of the different coefficients.

The results from this model are presented in Fig. 4 for a field with vertical polarization and in Fig. 5 for a field with horizontal polarization. Since the optical properties of Ag_2Ga are not very well known [42], all calculations have been performed for a gold-coated nanowire, under the assumption that the effects due to the presence of a different substance at the core could be ignored. These results are only meant for a qualitative analysis aimed at obtaining an order-of-magnitude estimate of the scattering forces and understanding the main directions of the scattered light. The spatial distribution of the scattered field shows a predisposition for backward-scattering, though with quite a wide angle. This is particularly prominent for vertically polarized light, but it holds generally true in other cases as well. It should not be surprising, then, that the most effective procedure for optical detection uses light ‘reflected’ back from the nanowire, although the potential for this (or any other) technique is limited by the aperture and light collecting ability of the setup. Alternatively, one could resort to the ‘transmission’ line instead, looking at the information obtainable from the absence of light in the form of the modulation of the diffracted shadow. Whilst less efficient, this method is not incompatible with the previous one and may be carried out concurrently. As we will see in more detail in the next paragraph, the two detection methods actually address different modes, corresponding to oscillations along orthogonal directions. Looking at the forces acting on the nanowire from Fig. 4a and Fig. 5a, we see that independently of wavelength or polarization the direct absorption forces are a couple of orders of magnitude smaller than the scattering forces. The model suggests fluctuating values of the forces depending on the radius of the nanowire (an effect less obvious for absorption forces due to the logarithmic scale). The positions and amplitudes of the local minima and maxima depend on the wavelength, creating situations in which the scattering force is, for example, stronger for 780 nm rather than 1064 nm. Therefore, depending on the geometry of the nanowire, one wavelength is more suitable for detection while the other is better for external control, as one applies a weaker back action and the other

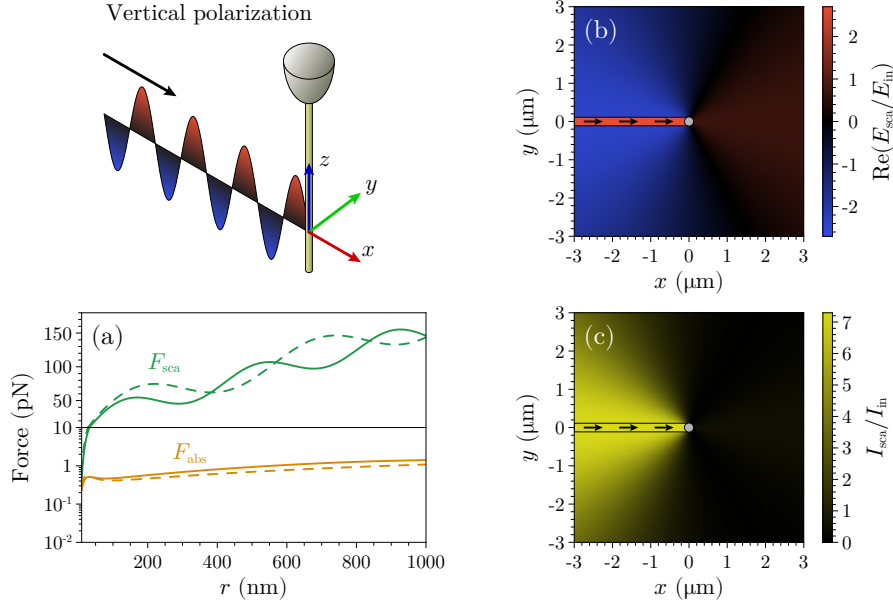


Figure 4: Scattering properties of a nanowire irradiated by a field with polarization parallel to the shaft. The nanowire is assumed to consist entirely of gold, with refractive index $n_{\text{nw}} = 0.2 + 4.8i$ ($0.2 + 7.0i$) for 780 nm (1064 nm) light. The refractive index of the medium, n_0 , is taken to be 1 regardless of whether the nanowire is in air or in vacuum. **(a)** Forces due to scattering (green) and absorption (orange) as a function of the radius of the nanowire, calculated according to Eq. 9–10. The traces are plotted for a beam of width $W = 10 \mu\text{m}$, power of 50 mW, and a wavelength of 780 nm (continuous) or 1064 nm (dashed). **(b–c)** Angular distribution of the scattered field and its intensity, as calculated from Eq. 4. The nanowire is placed at the origin and is assumed to have a radius of 120 nm. The incident light, of wavelength $\lambda = 780 \text{ nm}$, is approaching from the negative x axis. Its colour is adjusted to the maximum value of the scale rather than normalized to 1 in order to reveal the polarization at a glance.

exerts stronger forces. Even though direct absorption forces are relatively small, the indirect effect of photothermal absorption can have much more dramatic consequences than radiation pressure. Optically induced thermal bending of the Au/Ag₂Ga bimorph nanowires generates a bolometric force which is crucial for the interaction. The bolometric forces observed are estimated to be about one hundred times stronger than the radiation pressure

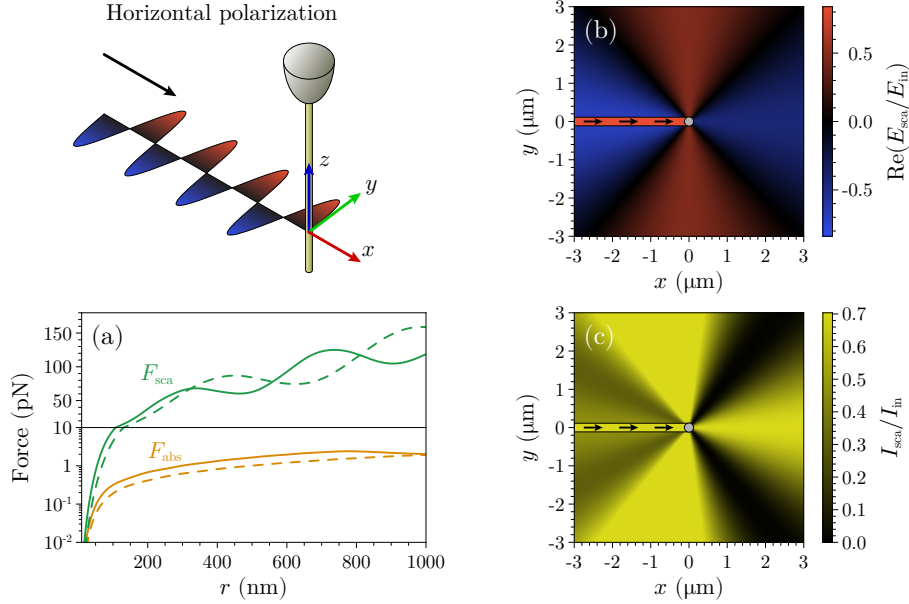


Figure 5: Scattering properties of a nanowire irradiated by a field with polarization normal to the shaft. The parameters used are the same as Fig. 4. **(a)** Forces due to scattering (green) and absorption (orange) as a function of the radius of the nanowire, for a wavelength of 780 nm (continuous) or 1064 nm (dashed). **(b–c)** Angular distribution of the scattered field and its intensity, for incident light of wavelength $\lambda = 780$ nm.

forces estimated by the model.

After interaction of the light with the nanowire, the light can be measured with various methods to obtain information about the nanowire vibrations. The modes of the nanowire appear in pairs, corresponding to the two motional eigenfrequencies in the plane orthogonal to the cylinder's axis. The slight difference in frequency of each mode originates from imperfections and asymmetries of the nanowire. To detect the vibrations we use two complementary methods applied to the same probe beam. In one method, a split photodiode measures the differences of the diffracted shadow in the transmitted light. Subtracting the photocurrents of the two pixels returns a modulated signal which corresponds to the nanowire fluctuations in the plane orthogonal to the direction of the light propagation. The other method, inspired by Doppler vibrometry [44], measures the change in phase of the light scattered back by the nanowire by comparing it with a refer-

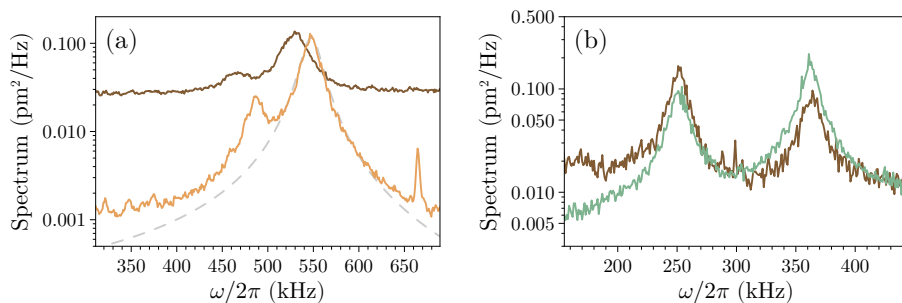


Figure 6: Spectra of the nanowires' thermal fluctuations. All traces have been recorded in ambient conditions. **(a)** Eigenmodes of a nanowire ($\approx 60 \mu\text{m}$ long, $\approx 350 \text{ nm}$ thick, gold-coated) obtained by interferometry on reflection, once with heterodyne (dark trace) and once with homodyne (light trace). Between the two measurements the nanowire may have been repositioned with a slightly different orientation, accounting for a small variation in the detection ratio of the two modes, and a permanent change was induced by the use of high power, slightly shifting both frequencies. The dashed trace follows the modelled displacement spectrum for an oscillator at room temperature with parameters similar to the measured ones. **(b)** Comparison between the two different detection method: interferometry on reflection (brown) and intensity subtraction from different pixels on transmission (green). The measurements were performed at the same time, and the difference in ratio between the peaks is due to the fact that the two methods have preferential directions of detection. The nanowire is uncoated, $\approx 40 \mu\text{m}$ in length and $\approx 270 \text{ nm}$ in diameter.

ence beam. This interferometric technique, which collects information on the oscillation along the same direction as the optical axis, proved to be the most practical and efficient. Choosing homodyne over heterodyne detection opens the possibility of phase-locking the interferometer, eliminating any loss of information due to averaging of the beating between the two beams. The two methods are compared in Fig. 6b.

4 Feedback control

Due to the non-directional Mie scattering from the nanowire, the effective radiation pressure force on the nanowire is small. The dominant optical force on the nanowire in our system is the photothermal bolometric force, estimated to be around one hundred times bigger than the radiation pressure force. The bolometric force is an indirect consequence of optical absorption,

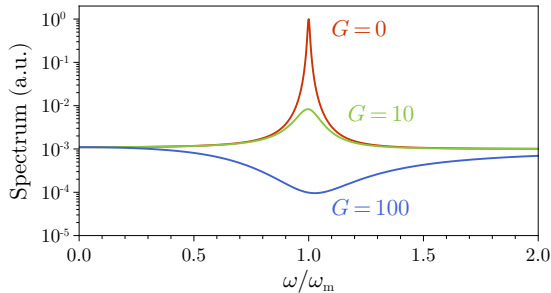


Figure 7: Theoretical displacement spectra indicative of feedback cooling, for an oscillator with quality factor $Q = 100$. All traces are normalized relative to the value of the spectrum at resonance and with no feedback, and the measurement noise is assumed to be 1000 times smaller than the thermally driven fluctuations.

arising from the thermal stress and deformation due to the change in temperature. It is particularly consequential for bimorph structures [45, 46], where a local increase in temperature induces thermal deflection of different materials at different rates [47].

While radiation pressure force is almost instantaneous, photothermal forces are typically slow due to the finite thermal conductivity of bulk materials. Nanostructures, however, can exhibit significantly faster response times compared to the bulk structures [48, 49]. Depending on the radius of the nanowire, r , and the thermal diffusivity, κ , the response time $\tau_c \simeq r^2/(4\kappa)$ [50] (required for the central temperature of a local Gaussian temperature distribution to decrease by 50%) can be as fast as few nanoseconds. This implies a response faster than the mechanical vibrations, which are typically slower than one megahertz. The heat generated by the laser light focused on a small area of the nanowire surface is sufficient to deflect the entire structure [47] faster than period of one mechanical oscillation. Therefore, modulating the intensity of the laser light can drive or suppress structural vibrations. The bolometric force may therefore be reliably employed for feedback control purposes. Unintuitively, the fast thermal response time of the nanowires enables the suppression of thermal fluctuations by thermal excitation.

Directing our attention to the case of purely negative feedback, we can study the effect of laser-induced damping and cooling of the system. The effective temperature of a vibrational mode, T_{eff} , is related to the measured spectral density of the fluctuations by the equipartition theorem. Under the effects of active control, in the regime of small feedback gains, the effective

temperature is given by

$$T_{\text{eff}} = \frac{T}{1 + G}, \quad (12)$$

where T is the initial temperature of the bath and G is the feedback gain [51, 52]. The feedback force is equivalent to an apparatus that has an effective damping $(1 + G)\gamma_m$, reducing the thermal excitations. Here, γ_m is the mechanical dissipation rate of the vibrations in the absence of feedback. For high gain, however, a full treatment of the problem taking into account the detection noise is required. In that regime, it can be shown [53] that the mode temperature is

$$T_{\text{eff}} = \frac{T}{1 + G} + \frac{m\omega_m^3}{4k_B Q} \frac{G^2}{1 + G} S_{\text{fb}}, \quad (13)$$

where m , ω_m are the effective mass and the oscillation frequency of the nanowire, k_B is the Boltzmann constant and S_{fb} is the noise floor of the displacement measurement, which also modulates the nanowire's motion through the feedback loop. This result shows that the feedback gain cannot be turned up indefinitely to reduce the effective temperature [53]. Therefore, the minimum temperature that can be achieved through feedback cooling by optimizing the gain depends on the measurement noise as

$$T_{\text{eff}}^{(\text{min})} = \sqrt{\frac{Tm\omega_m^3 S_{\text{fb}}}{k_B Q}}. \quad (14)$$

It should be noted that this results from a purely classical argument. To reach the quantum state of the system with active control, it is fundamental for the feedback to operate with quantum-limited detection and to propagate non-classical states [54].

4.1 Experimental results

In this section we describe results of nanowire detection and its photothermal cooling. Operations on the nanowires have been performed using a two-stage scheme: one part for the detection of the thermally driven modes, one part for the realization of feedback control. The simplified diagram of Fig. 8 shows how the two different roles are performed by separate lasers. The requirement for independent sources comes primarily from the necessity of having the beams co-propagate without interference, and the wavelength of each laser is, in itself, only a secondary requirement. The absorption and

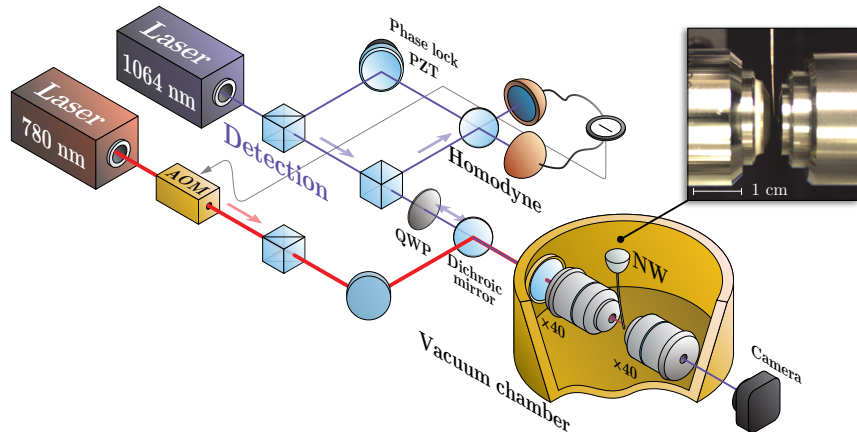


Figure 8: Comprehensive scheme of the experiment on the nanowire (NW). The two optical branches are used for the detection of the thermal motion of the nanowire (1064 nm) and for the feedback control to suppress the thermal fluctuations (780 nm). The inset shows a close-up photograph of the tungsten needle with the nanowire at its tip, between two microscope objective lenses.

scattering properties of the nanowires are, of course, elements that need to be considered for an appropriate choice of the operating wavelengths. The detection branch is powered by a 1064 nm beam, while light around 780 nm is used for the actuation, largely because the nanowire under investigation displayed a stronger response in the near infrared and better resistance to high power at longer wavelengths. The vacuum chamber, where the nanowire and the two focusing microscope objective lenses are located, is maintained by an ion pump at pressures of 10^{-5} – 10^{-4} Pa, occasionally observed to go down to the 10^{-6} Pa range. A vacuum-compatible nano-positioning stage is used to allow alignment within the enclosed chamber. In the feedback branch, control on the nanowire’s motion is realized by an acousto-optic modulator (AOM) that varies the amplitude of the field and the consequent back-action on the oscillator. The AOM is driven in real time by a signal extracted from the detection scheme, after appropriate processing required to achieve the desired gain and phase for the feedback.

Examples of the spectral response of the nanowire when subject to feedback cooling are shown in Fig. 9. Feedback control can cool the nanowire’s modes both individually and collectively. The practical limits of cold damping imposed by the measurement noise are reached with single-mode cooling, and, for high gain, squashing is observed [55] (cf. Fig. 9a). For multi-mode

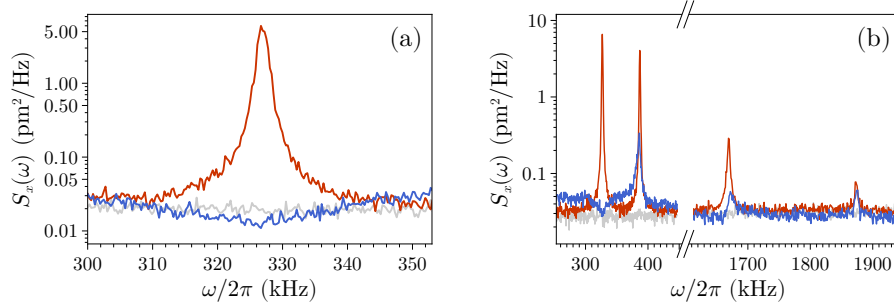


Figure 9: Displacement spectra of a nanowire subject to feedback cooling. The nanowire is $\approx 60\ \mu\text{m}$ in length, $\approx 220\ \text{nm}$ in diameter, and is gold coated. **(a)** Single-mode cooling. The amplitude of the thermal fluctuations (red) is suppressed down to the level of the background noise and beyond (blue), giving rise to squashing in the displacement spectrum. The grey trace indicates the detection noise in the absence of the nanowire. **(b)** Multi-mode cooling. The parameters of the feedback are optimized towards cooling of the mode with the lowest frequency, although in order to obtain cooling of the higher-order modes the phase of the feedback cannot be adjusted optimally and more measurement noise is injected into the system.

cooling, besides the detection efficiency there are further limits set by the bandwidth of the feedback and more importantly the ability to control its phase across a wide spectrum of frequencies. The technical constraint to the bandwidth scales as the inverse of the characteristic response time τ_{th} , and is not found to be significant relative to the nanowire's modes. On the other hand, the feedback phase needs to be precisely tuned in order to achieve pure damping. Fine adjustments are only possible over a relatively small frequency range, and pushing more than one mode to the coldest temperature at the same time would only be feasible with the introduction of more advanced controls. Nevertheless, as Fig. 9b shows, the feedback implemented is capable of cooling simultaneously modes spanning up to 2 MHz.

Figure 10 shows the temperature of the fundamental oscillation modes of the nanowire as a function of the feedback gain applied to cool the thermal vibrations. The results vary considerably depending on whether the nanowire is in ambient or in vacuum conditions, highlighting the importance of a high quality factor for improved results. At atmospheric pressures, the additional dissipation due to the viscosity of the air molecules implies that more power is required to achieve the same levels of actuation obtained in vacuum. At low pressure the quality factor of the oscillations is much higher,

rendering the entire procedure more effective. Starting from a room temperature of 293 K, the lowest single-mode temperature attained is 17.4(2) K. In air it was only possible to cool down to 49(5) K. It should be noted that, even under similar pressure conditions, different modes respond to feedback at different rates and one may be cooled more rapidly than the other. The degree of influence is determined by the spatial overlap of the modes with the direction of the bolometric actuation, which does not depend on the orientation relative to the feedback beam. The reduction in temperature and thermal fluctuations achieved is sufficient to increase the measurement sensitivity of the nanowire to impulsive forces [34].

The results of Fig. 9 and 10 are primarily limited by the feedback of detection noise into the system and efficiency of the overall control loop. The gain at which the effective temperature corresponds to its minimum value corresponds to the turning point where the measured spectrum shifts from cold damping to squashing [55] (see Fig. 7).

5 Discussion and possible improvements

A higher quality factor or a thermal bath at lower temperatures, such as in cryogenic conditions, could push the minimum temperature attainable by the feedback to lower limits. Ultimately, however, the results of Fig. 10 are limited by the feedback of detection noise into the system and the efficiency of the overall control loop.

Cooling of the mechanical resonator to its lowest energy state is only possible with feedback when the measurement sensitivity is increased to be near the standard quantum limit [54, 56]. This can only be achieved by enhancing the typically weak interaction of the optical field with the mechanical mode of interest. For this reason each photon should be contained within a small volume (V), for example by having the nanowire interact with a miniaturized optical resonator. Micro- and nanophotonic structures are capable of reducing the interaction mode volume to values on the order of λ^3 [57, 40]. However, going beyond this regime is not possible with conventional nanophotonics due to the diffraction limit.

Alternatively, optomechanical interaction can be enhanced using plasmonic confinement of light. To push the coupling strength beyond what is achievable by conventional nano-optomechanical systems, one can use the metallic properties of the nanowire to take advantage of plasmonic resonances, effectively confining the optical mode below the diffraction limit. To use the plasmon-enhanced absorption to our advantage, the system should

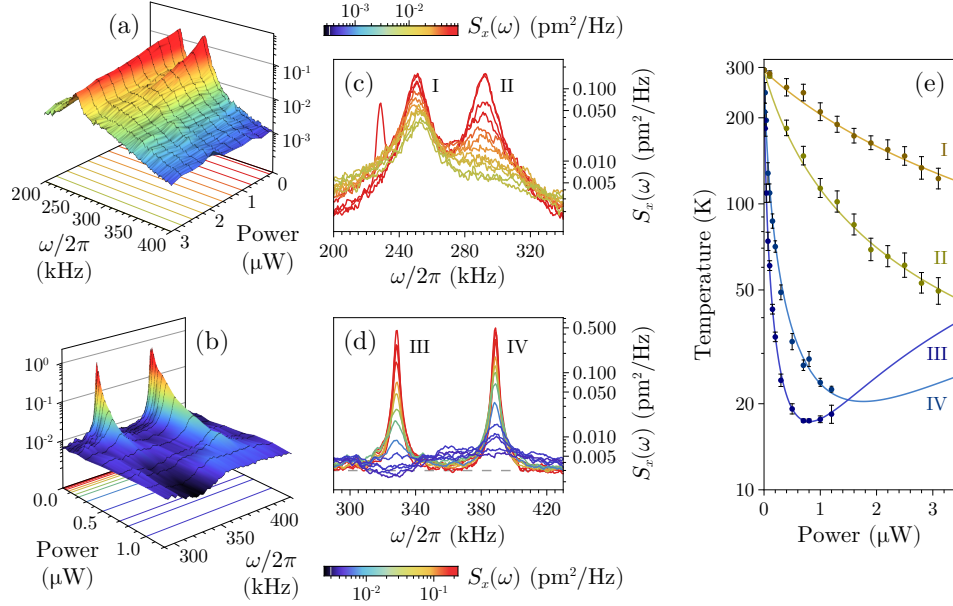


Figure 10: Proof-of-principle experimental result demonstrating thermal noise reduction of a nanowire as a function of gain, which is controlled by the power of the feedback beam. The nanowire used in atmospheric conditions is gold-coated, $\approx 50 \mu\text{m}$ in length and $\approx 300 \text{ nm}$ in diameter. The nanowire used in vacuum conditions is the same as Fig. 9. **(a–b)** Spectrum of the thermal fluctuations for increasing power, in air (a) and in vacuum (b). The black mesh lines represent the individual traces, projected onto the bottom face with a colour corresponding to the peak value of the coldest mode. The detection noise level is indicated in the colour gradient scale by a grey line. **(c–d)** Front view of the spectra in (a–b), colour-coded according to the peak value of the coldest mode (“II” in air, “III” in vacuum). **(e)** The temperature of each mode, calculated according to Eq. 13. The error bars are estimated by propagating the uncertainty in the Lorentzian fit of the amplitude noise. The solid lines are theoretical fits assuming a linear relationship between the optical power of the feedback beam and the overall feedback gain. The resulting conversion factors between power and gain estimated for the four modes are $0.4 \mu\text{W}^{-1}$ (I), $1.6 \mu\text{W}^{-1}$ (II), $39.3 \mu\text{W}^{-1}$ (III), and $15.1 \mu\text{W}^{-1}$ (IV).

be engineered to favour photothermal interaction over scattering forces. In this way, it would be possible to achieve coupling strengths orders of magnitude larger than those achieved via radiation pressure forces [58, 59].

The plasmon effect in our system can be quantified by modelling the

scattering and absorption cross sections of the nanowire defined as $\sigma^{\text{sca}} = P_{\text{sca}}/I_{\text{in}}$ and $\sigma^{\text{abs}} = P_{\text{abs}}/I_{\text{in}}$ respectively, where P_{sca} and P_{abs} are the scattered and absorbed power and I_{in} is the intensity of the incident field. These cross sections are related to the scattering and absorption efficiencies (cf. Eq. 7–8) and can be obtained by multiplying the corresponding quantity by the cross-sectional area of the nanowire. Therefore, in long nanowires the total value of the cross sections can be represented as a superposition of cylindrical modes. This decomposition can generally be represented as $\sigma^{\text{sca/abs}} = \sum_{n=-\infty}^{+\infty} \sigma_n^{\text{sca/abs}}$, in which $\sigma_n^{\text{sca/abs}}$ is a single-mode scattering or absorption cross section (positive and negative order harmonics) and n is the mode number [41]. In a single nanowire, the mode degeneracy of the positive and negative orders appears due to the azimuthal symmetry. The spectral behaviour of every mode is a function of size and material parameters of the nanowire.

Here we consider the small-size effect in plasmonic materials which may have dielectric constants quite different from those of bulk materials. Confinement of the electrons' motion in conductive nanowires is more significant when the diameter is comparable to the mean free path of the electrons in bulk material, requiring the collision frequency to be modified. This causes a variation of the nanowire's conductivity and optical properties due to the strong influence of the surface. In thinner nanowires, the electrons reach the surface faster and cause an increase in the scattering rate [60, 61].

To take this size-dependent effect into account, we calculate the correction to the dielectric permittivity using Drude's model,

$$\epsilon = \epsilon_{\infty} - \frac{\omega_p^2}{\omega^2 + i\gamma\omega}, \quad (15)$$

where $\omega = 2\pi c/\lambda$ is the optical angular frequency, ω_p and γ are the plasma angular frequency and the electron collision frequency [62], and ϵ_{∞} is the relative permittivity in bulk material at high frequencies, in which case electrons cannot follow the excitation. To consider the small-size effect, we replace the collision frequency γ with one that accounts for the small dimensions of the object, $\gamma_{\text{nw}} = \gamma_{\text{bulk}} + Av_F/d$, where $A = 1$, v_F is the Fermi velocity, and d is the characteristic size of the metallic structure (in this case, the thickness of the plasmonic cell) [60, 61]. To obtain the corrected dielectric permittivity of metals in the nanostructure using experimental data, first we use the real and imaginary parts of the bulk material's permittivity

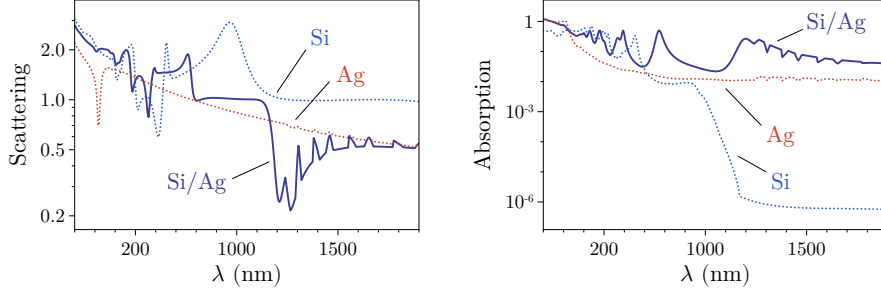


Figure 11: Calculated scattering and absorption cross sections as a function of wavelength of the incident light for three nanowires: silver (Ag), silicon (Si, a non-plasmonic material as reference), and a core/shell Si/Ag structure. The radius of the silver and the silicon nanowires is, in both cases, 100 nm. The plasmonic shell of silver, with a thickness of 20 nm, is added to the 100-nm silicon nanowire to reveal the effects of the plasmonic coating on a dielectric nanowire. The cross sections, calculated in two-dimensional simulations, are expressed in unit length of the nanowires and are normalized relative to $2\lambda/\pi$.

to achieve exact γ_{bulk} and ω_{p} , using Drude's formula as follows:

$$\gamma_{\text{bulk}} = \frac{\omega \Im(\epsilon)}{(\epsilon_{\infty} - \Re(\epsilon))}, \quad \omega_{\text{p}}^2 = \omega^2 \frac{(\epsilon_{\infty} - \Re(\epsilon))^2 + \Im(\epsilon)^2}{\epsilon_{\infty} - \Re(\epsilon)}. \quad (16)$$

Then, by calculating γ_{nw} and using it in Drude's model, we recover the value of ϵ (one also can use the approximation $\epsilon_{\text{nw}} = \epsilon_{\text{bulk}} + i[\omega_{\text{p}}^2 v_{\text{F}}]/[\omega^3 d]$). For longer wavelengths these discrepancies can be reduced by using appropriate values of ϵ_{∞} , γ_{bulk} and ω_{p} . Calculated absorption and scattering cross sections are plotted in Fig. 11 for Ag and Si nanowires as a function of the wavelength of the incident beam. The parameters used in Drude's model for silver are: $\epsilon_{\infty} = 1$, $\omega_{\text{p}} = 2\pi \times 2.18$ PHz, and $\gamma = 2\pi \times 4.353$ THz.

The simulation results show that metallic nanowires or general metal coated optomechanical structures can be tuned close to their plasmonic modes by appropriate choice of laser wavelength to obtain a hybrid plasmon-optomechanical system. In particular, the detection can be improved by choosing a wavelength favouring scattering over absorption, while the actuation can be enhanced by choosing a wavelength at which most of the energy is absorbed rather than dispersed with the scattered field. As shown in Fig. 11, this complementary response can even be engineered on non-plasmonic systems, such as silicon nanowires, by introducing an appropriate metal coating. Increased absorption can also be realized by tailoring a

multi-layered structure on the nanowire [63]. These novel systems offer a new regime of light-matter interaction, capable of reaching optomechanical interaction strengths much larger than what is available with the current systems [58]. Also, the broadband plasmonic interaction is not related to the enhancement obtained when coupling the oscillator to a nanocavity, and it can be used to introduce additional Purcell enhancement [64].

There are, however, typically two main difficulties in using conventional plasmonic systems for quantum experiments: firstly, the plasmonic materials introduce enhanced incoherent absorption and therefore losses; secondly, the metallic structures containing highly confined plasmonic modes suffer from weak coupling to the far field. The loss in plasmonic structures is almost unavoidable, and it has been theoretically shown that the dispersive coupling for the lateral motion of the plasmonic structure is negligible compared to the dissipative coupling [65]. Unconventionally, we propose using the dissipative coupling which results in localized heating to our advantage, by engineering a system where photothermal forces are the dominant type of optomechanical interaction, as described above. On the other hand, the weak coupling to the far field can be resolved by interfacing the metallic nanowires with nanophotonic structures [40]. Proper design of the structure may lead to optomechanical coupling strength as high as 2 THz nm^{-1} [58].

6 Towards quantum ground state cooling

Indulging in speculation, we regard the possibility of reaching the quantum regime of the modes of a mechanical oscillator by deliberate heating. A realistic outlook would comprise enhanced interaction and detection capabilities at the quantum limit. We envision a system where the tip of a Si nanowire is placed inside the evanescent mode of a nanophotonic cavity confining the probe beam (of wavelength $\lambda_p \approx 1000 \text{ nm}$) to amplify the signal-to-noise ratio of the measurement. In this scheme, the control beam (of wavelength $\lambda_c \approx 300 \text{ nm}$) impinges on a small region of the nanowire away from the tip where the nanowire is coated with silver. The small interaction volume provided by the nanophotonic structure can reduce the noise floor of the displacement measurement to sub-fm $\text{Hz}^{-1/2}$ as previously demonstrated [66]. This is close to the quantum zero-point fluctuations of the oscillator represented by $x_{\text{ZPF}} = \sqrt{\hbar/(2m\omega_m)}$, where \hbar is the Planck constant. By additionally choosing the probe and control wavelengths to respectively coincide with plasmonic resonances for scattering and absorption, the nanowire position can be measured to its ultimate precision limit

and its thermal motion can be suppressed with high accuracy to allow, in principle, cooling of the vibrational modes of a nanomechanical oscillator near the QGS.

The temperature required to obtain a mean phonon occupation number $n_m = (e^{\frac{\hbar\omega_m}{k_B T}} - 1)^{-1}$ less than one, and therefore reach the QGS of the oscillator, is estimated to be about 10 μ K for a vibrational frequency of 200 kHz. Taking into account the strong feedback force and a displacement measurement at the quantum limit, an oscillator with a mass of 10 pg and a moderate quality factor of 10^4 is capable of reaching the vibrational QGS. For example, starting from a cryogenic temperature of 4 K, a phonon occupation number of 10 can be obtained with a displacement noise spectral density of about 0.1 fm Hz^{-1/2}, and less than 1 phonon is obtained at 0.01 fm Hz^{-1/2}. Nevertheless, one may demand a higher quality factor not only to facilitate the process but also to improve the coherence of the system. The number of coherent oscillations before the assimilation of a phonon from the thermal environment is dictated by the product of the quality factor and the frequency of the oscillation as $Q \cdot \omega_m \times \hbar / (k_B T)$ [67, 24]. With a cryogenic bath and the sub-megahertz frequency considered, a quality factor greater than 4×10^5 is required to maintain the coherence in the system for more than one oscillation. In this regime, quantum sensing of impulsive external forces is enabled even at low frequencies.

Acknowledgements

This research is supported by the Australian Research Council Centre of Excellences CE110001027, the Discovery Project DP150101035. PKL is supported by the ARC Laureate Fellowship FL150100019, BCB by the ARC Future Fellowship FT100100048.

References

- [1] Imboden, M. and Mohanty, P., “Dissipation in nanoelectromechanical systems”, *Physics Reports* **534** 89–146 (2014).
- [2] Dong, M., Husale, S., and Sahin, O., “Determination of protein structural flexibility by microsecond force spectroscopy”, *Nature Nanotechnology* **4** 514–517 (2009).

- [3] Burg, T. P., Godin, M., Knudsen, S. M. et al., “Weighing of biomolecules, single cells and single nanoparticles in fluid”, *Nature* **446** 1066–1069 (2007).
- [4] Naik, A. K., Hanay, M. S., Hiebert, W. K. et al., “Towards single-molecule nanomechanical mass spectrometry”, *Nature Nanotechnology* **4** 445–450 (2009).
- [5] Li, M., Myers, E. B., Tang, H. X. et al., “Nanoelectromechanical resonator arrays for ultrafast, gas-phase chromatographic chemical analysis”, *Nano Letters* **10** 3899–3903 (2010).
- [6] Gil-Santos, E., Ramos, D., Martínez, J. et al., “Nanomechanical mass sensing and stiffness spectrometry based on two-dimensional vibrations of resonant nanowires”, *Nature Nanotechnology* **5** 641–645 (2010).
- [7] Mamin, H. J. and Rugar, D., “Sub-attoneutron force detection at millikelvin temperatures”, *Applied Physics Letters* **79**, 20 (2001).
- [8] Liu, C.-H., Barzilai, A. M., Reynolds, J. K. et al., “Characterization of a High-Sensitivity Micromachined Tunneling Accelerometer with Microg Resolution”, *Journal of Microelectromechanical Systems* **7**, 2 235–244 (1998).
- [9] Cleland, A. N. and Roukes, M. L., “A nanometre-scale mechanical electrometer”, *Nature* **392** 160–162 (1998).
- [10] Rugar, D., Budaklan, R., Mamin, H. J. et al., “Single spin detection by magnetic resonance force microscopy”, *Nature* **430** 329–332 (2004).
- [11] Ekinici, K. L. and Roukes, M. L., “Nanoelectromechanical systems”, *Review of Scientific Instruments* **76**, 061101 (2005).
- [12] Aspelmeyer, M., Meystre, P., and Schwab, K. C., “Quantum optomechanics”, *Physics Today* **65**, 7 29 (2012).
- [13] Poot, M. and van der Zant, H. S. J., “Mechanical systems in the quantum regime”, *Physics Reports* **511** 273–335 (2012).
- [14] Verhagen, E., Deléglise, S., Weis, S. et al., “Quantum-coherent coupling of a mechanical oscillator to an optical cavity mode”, *Nature* **482** 63–67 (2012).

- [15] O’Connell, A. D., Hofheinz, M., Ansmann, M. et al., “Quantum ground state and single-phonon control of a mechanical resonator”, *Nature* **464** 697–703 (2010).
- [16] Teufel, J. D., Donner, T., Li, D. et al., “Sideband cooling of micromechanical motion to the quantum ground state”, *Nature* **475** 359–363 (2011).
- [17] Chan, J., Mayer Alegre, T. P., Safavi-Naeini, A. H. et al., “Laser cooling of a nanomechanical oscillator into its quantum ground state”, *Nature* **478** 89–92 (2011).
- [18] Brooks, D. W. C., Botter, T., Schreppler, S. et al., “Non-classical light generated by quantum-noise-driven cavity optomechanics”, *Nature* **488** 476–480 (2012).
- [19] Safavi-Naeini, A. H., Gröblacher, S., Hill, J. T. et al., “Squeezed light from a silicon micromechanical resonator”, *Nature* **500** 185–189 (2013).
- [20] Purdy, T. P., Yu, P.-L., Peterson, R. W. et al., “Strong Optomechanical Squeezing of Light”, *Physical Review X* **3**, 031012 (2013).
- [21] Palomaki, T. A., Harlow, J. W., Teufel, J. D. et al., “Coherent state transfer between itinerant microwave fields and a mechanical oscillator”, *Nature* **495** 210–214 (2013).
- [22] Miao, H., Danilishin, S. L., Müller-Ebhardt, H. et al., “Achieving ground state and enhancing optomechanical entanglement by recovering information”, *New Journal of Physics* **12**, 083032 (2010).
- [23] Miao, H., Danilishin, S. L., Müller-Ebhardt, H. et al., “Probing macroscopic quantum states with a sub-Heisenberg accuracy”, *Physical Review A* **81**, 012114 (2010).
- [24] Norte, R. A., Moura, J. P., and Gröblacher, S., “Mechanical Resonators for Quantum Optomechanics Experiments at Room Temperature”, *Physical Review Letters* **116**, 147202 (2016).
- [25] Metzger, C. and Karrai, K., “Cavity cooling of a microlever”, *Nature* **432** 1002–1005 (2004).
- [26] Metzger, C., Favero, I., Ortlieb, A. et al., “Optical self cooling of a deformable Fabry-Perot cavity in the classical limit”, *Physical Review B* **78**, 035309 (2008).

- [27] De Liberato, S., Lambert, N., and Nori, F., “Quantum noise in photothermal cooling”, *Physical Review A* **83**, 033809 (2011).
- [28] Restrepo, J., Gabelli, J., Ciuti, C. et al., “Classical and quantum theory of photothermal cavity cooling of a mechanical oscillator”, *Comptes Rendus Physique* **12** 860–870 (2011).
- [29] Yazdanpanah, M. M., Harfenist, S. A., Safir, A. et al., “Selective self-assembly at room temperature of individual freestanding Ag₂Ga alloy nanoneedles”, *Journal of Applied Physics* **98**, 07 073510 (2005).
- [30] Yazdanpanah, M. M., Hosseini, M., Pabba, S. et al., “Micro-wilhelmy and related liquid property measurements using constant-diameter nanoneedle-tipped atomic force microscope probes”, *Langmuir* **24**, 23 13753–13764 (2008).
- [31] Zhao, M., Gu, X., Lowther, S. E. et al., “Subsurface characterization of carbon nanotubes in polymer composites via quantitative electric force microscopy”, *Nanotechnology* **21**, 225702 (2010).
- [32] Dobrokhotov, V. V., Yazdanpanah, M. M., Pabba, S. et al., “Visual force sensing with flexible nanowire buckling springs”, *Nanotechnology* **19**, 035502 (2008).
- [33] Gao, P. and Cai, Y., “Label-free detection of the aptamer binding on protein patterns using Kelvin probe force microscopy (KPFM)”, *Analytical and Bioanalytical Chemistry* **394**, 1 207–214 (2009).
- [34] Hosseini, M., Guccione, G., Slatyer, H. J. et al., “Multimode laser cooling and ultra-high sensitivity force sensing with nanowires”, *Nature Communications* **5**, 4663 (2014).
- [35] Chen, C., Ma, M., Zhe Liu, J. et al., “Viscous damping of nanobeam resonators: Humidity, thermal noise, and a paddling effect”, *Journal of Applied Physics* **110**, 034320 (2011).
- [36] Butt, H.-J. and Jaschke, M., “Calculation of thermal noise in atomic force microscopy”, *Nanotechnology* **6**, 1 1–7 (1995).
- [37] Newell, W. E., “Miniaturization of Tuning Forks”, *Science* **161**, 3848 1320–1326 (1968).
- [38] Chan, J., Eichenfield, M., Camacho, R. et al., “Optical and mechanical design of a “zipper” photonic crystal optomechanical cavity”, *Optics Express* **17**, 5 3802–3817 (2009).

- [39] Favero, I., Stapfner, S., Paulitschke, P. et al., “Fluctuating nanomechanical systems in a high finesse optical microcavity”, *Optics Express* **17**, 15 12813–12820 (2009).
- [40] Miura, R., Imamura, S., Ohta, R. et al., “Ultralow mode-volume photonic crystal nanobeam cavities for high-efficiency coupling to individual carbon nanotube emitters”, *Nature Communications* **5** 5580 (2014).
- [41] Bohren, C. F. and Huffman, D. R., *Absorption and Scattering of Light by Small Particles*, Wiley-VCH (2008).
- [42] Biedermann, L. B., “Vibrational Spectra of Nanowires Measured Using Laser Doppler Vibrometry and STM Studies of Epitaxial Graphene”, Technical report, Sandia National Laboratories (2009).
- [43] Svoboda, K. and Block, S. M., “Optical trapping of metallic Rayleigh particles”, *Optics Letters* **19**, 13 930–932 (1994).
- [44] Biedermann, L. B., Tung, R. C., Raman, A. et al., “Characterization of silver-gallium nanowires for force and mass sensing applications”, *Nanotechnology* **21**, 30 305701 (2010).
- [45] Metzger, C., Ludwig, M., Neuenhahn, C. et al., “Self-Induced Oscillations in an Optomechanical System Driven by Bolometric Backaction”, *Physical Review Letters* **101**, 133903 (2008).
- [46] Fu, H., Liu, C., Liu, Y. et al., “Selective photothermal self-excitation of mechanical modes of a micro-cantilever for force microscopy”, *Applied Physics Letters* **99**, 173501 (2011).
- [47] Ikuno, T., Honda, S., Yasuda, T. et al., “Thermally driven nanomechanical deflection of hybrid nanowires”, *Applied Physics Letters* **87**, 21 213104 (2005).
- [48] Dhara, S., Solanki, H. S., Ravikumar, A. P. et al., “Tunable thermal conductivity in defect engineered nanowires at low temperatures”, *Physical Review B* **84**, 121307(R) (2011).
- [49] Pradhan, N. R., “Thermal conductivity of nanowires, nanotubes and polymer-nanotube composites”, Ph.D. thesis, Worcester Polytechnic Institute (2010).
- [50] Anderson, R. R. and Parrish, J. A., “Selective Photothermolysis: Precise Microsurgery by Selective Absorption of Pulsed Radiation”, *Science* **220**, 4596 524–527 (1983).

- [51] Mancini, S., Vitali, D., and Tombesi, P., “Optomechanical Cooling of a Macroscopic Oscillator by Homodyne Feedback”, *Physical Review Letters* **80**, 4 688–691 (1998).
- [52] Pinard, M., Cohadon, P.-F., Briant, T. et al., “Full mechanical characterization of a cold damped mirror”, *Physical Review A* **63**, 01 013808 (2000).
- [53] Poggio, M., Degen, C. L., Mamin, H. J. et al., “Feedback Cooling of a Cantilever’s Fundamental Mode below 5 mK”, *Physical Review Letters* **99**, 017201 (2007).
- [54] Wiseman, H. M. and Milburn, G. J., “Quantum Theory of Optical Feedback via Homodyne Detection”, *Physical Review Letters* **70**, 5 548–551 (1993).
- [55] Buchler, B. C., Gray, M. B., Shaddock, D. A. et al., “Suppression of classic and quantum radiation pressure noise by electro-optic feedback”, *Optics Letters* **24**, 4 259–261 (1999).
- [56] Clerk, A. A., Devoret, M. H., Girvin, S. M. et al., “Introduction to quantum noise, measurement, and amplification”, *Reviews of Modern Physics* **82**, 2 1155–1208 (2010).
- [57] Anetsberger, G., Arcizet, O., Unterreithmeier, Q. P. et al., “Near-field cavity optomechanics with nanomechanical oscillators”, *Nature Physics* **5** 909–914 (2009).
- [58] Thijssen, R., Verhagen, E., Kippenberg, T. J. et al., “Plasmon Nanomechanical Coupling for Nanoscale Transduction”, *Nano Letters* **13** 3293–3297 (2013).
- [59] Thijssen, R., Kippenberg, T. J., Polman, A. et al., “Plasmomechanical Resonators Based on Dimer Nanoantennas”, *Nano Letters* **15** 3971–3976 (2015).
- [60] Kreibig, U., “Electronic properties of small silver particles: the optical constants and their temperature dependence”, *Journal of Physics F* **4** 999–1014 (1974).
- [61] Cao, G. and Wang, Y., *Nanostructures and Nanomaterials: Synthesis, Properties and Applications*, World Scientific, 2nd edition (2004).

- [62] Ordal, M. A., Bell, R. J., Alexander Jr, R. W. et al., “Optical properties of fourteen metals in the infrared and far infrared: Al, Co, Cu, Au, Fe, Pb, Mo, Ni, Pd, Pt, Ag, Ti, V, and W”, *Applied Optics* **24**, 24 4493–4499 (1985).
- [63] Mirzaei, A., Shadrivov, I. V., Miroschnichenko, A. E. et al., “Superabsorption of light by multilayer nanowires”, *Nanoscale* **7** 17658–17663 (2015).
- [64] van Exter, M. P., Nienhuis, G., and Woerdman, J. P., “Two simple expressions for the spontaneous emission factor ?”, *Physical Review A* **54**, 4 3553–3558 (1996).
- [65] Hassani nia, I. and Mohseni, H., “Surface-plasmon-polariton–assisted dissipative backaction cooling and amplification”, *Physical Review A* **92**, 053852 (2015).
- [66] Schliesser, A., Arcizet, O., Rivière, R. et al., “Resolved-sideband cooling and position measurement of a micromechanical oscillator close to the Heisenberg uncertainty limit”, *Nature Physics* **5** 509–514 (2009).
- [67] Nguyen, D. T., Baker, C., Hease, W. et al., “Ultrahigh Q-frequency product for optomechanical disk resonators with a mechanical shield”, *Applied Physics Letters* **103**, 241112 (2013).